

Anisotropic exchange interaction between nonmagnetic europium cations in Eu_2O_3 G. Concas,^{1,*} J. K. Dewhurst,² A. Sanna,² S. Sharma,² and S. Massidda³¹*Dipartimento di Fisica, Università degli Studi di Cagliari, and INSTM, S.P. Monserrato-Sestu km 0.700, I-09042 Monserrato (CA), Italy*²*Max-Planck-Institut für Mikrostrukturphysik, Weinberg 2, D-06120 Halle, Germany*³*CNR-IOM SLACS, and Dipartimento di Fisica, Università degli Studi di Cagliari, S.P. Monserrato-Sestu km 0.700, I-09042 Monserrato (CA), Italy*

(Received 9 March 2011; revised manuscript received 25 May 2011; published 28 July 2011; publisher error corrected 2 August 2011)

The electronic structure of the cubic and (high pressure) hexagonal phases of Eu_2O_3 have been investigated by means of full potential linearized augmented plane wave calculations, within the LDA + U method. A full structural relaxation was performed for both phases, and the transition pressure was determined. The band structure shows the correct insulating character with gap values comparable to the experimental ones. The contact charge density was also calculated for Eu_2O_3 (and other Eu compounds) and found to be in good agreement with experimental values. For the cubic phase, the comparison between ferromagnetic and antiferromagnetic calculations shows that the exchange interaction is very weak and is therefore expected to have a negligible effect on the magnetic susceptibility. The calculations performed for the high pressure hexagonal phase, on the other hand, show that there is an antiferromagnetic exchange interaction between nearest-neighbor Eu ions, which should have a sizable effect on the susceptibility. Our results allow us to evaluate the existing theories.

DOI: [10.1103/PhysRevB.84.014427](https://doi.org/10.1103/PhysRevB.84.014427)

PACS number(s): 75.20.Ck, 75.30.Et, 71.15.Mb, 71.20.Ps

I. INTRODUCTION

Rare earth compounds present a large variety of interesting magnetic behaviors, due to their partially filled f shells. Trivalent europium compounds, in particular, offer a unique chance of observing exchange coupling between “nonmagnetic” ions. The ground state of Eu^{3+} ($4f^6$) ions is 7F_0 , with a total angular momentum $J = 0$ resulting from $L = S = 3$ (in atomic units) although spin-dependent exchange effects are present. Eu ions also show a substantial admixture of higher energy $J = 1$ states, which contributes significantly to their susceptibility (χ).

Eu_2O_3 is the prototypical compound of this family, its magnetic susceptibility has been the subject of detailed experimental investigation.^{1–3} The first attempt to explain its magnetic behavior was made by Huang and Van Vleck,⁴ who showed that the susceptibility of Eu_2O_3 is larger than the corresponding susceptibility of the free Eu^{3+} ion, because the energy levels of the excited 7F_1 states are modified by the crystal field, and pointed out the dominant contribution of the Van Vleck component of the susceptibility, χ_{VV} . An explicit calculation of the susceptibility from energy levels obtained by optical spectroscopy measurements^{5,6} was performed in this work. However, the resulting χ turned to be smaller than the experimental value, and so the remainder was attributed entirely to the exchange coupling among Eu^{3+} ions.⁴

This viewpoint has been challenged on the basis of measurements of χ in solid solutions of Eu_2O_3 into A_2O_3 ($A = \text{Y}, \text{Lu}, \text{Sc}$),^{2,3,7,8} where Eu atoms are diluted. As the number of Eu nearest neighbors is reduced, the total interatomic exchange interaction should decrease and become negligible at small concentrations of Eu, and the total susceptibility should decrease along with it. The experimental susceptibility (per mole of Eu), however, does not decrease in the full range of investigation [i.e., up to 10% of Eu_2O_3 into A_2O_3 (Refs. 2, 3, 7, and 8)], suggesting a negligible role of the exchange interaction. This decrease of the exchange component on dilution might be due to compensation caused by change in

the crystal field splitting of Eu sites in A_2O_3 in comparison with Eu_2O_3 ; this explanation, however, is not supported by optical measurements of the energy levels.^{6,9,10} Yet another explanation has been proposed based on the distribution of Eu atoms in the two available sites (symmetry S_6 and C_2) of the cubic bixbyite structure of these oxides.¹¹ The decrease of the exchange component on dilution might be compensated by a preferential occupation of the S_6 site in the solid solution; the Van Vleck susceptibility of this site is larger because the 7F_1 levels are lower in energy in comparison with the C_2 site. This preferential occupation, however, was not found in X-ray diffraction² or Mössbauer spectroscopic studies.^{3,12}

A further criticism to the viewpoint that the exchange coupling guides the physics of susceptibility also comes from the calculations of the Van Vleck susceptibility performed by Caro and Porcher.¹³ These authors determined the crystalline field parameters starting from the experimental values of the energies of the excited states, and the matrix elements of the Van Vleck susceptibility were calculated using this potential and the atomic functions. The susceptibility calculated accordingly agrees well with the experimental one,¹ validating a picture in which the exchange coupling should be negligible. We should mention here, however, that the optical data used by Caro and Porcher have been subsequently corrected by more recent measurements.⁶

Therefore, the question of whether the excess of susceptibility may be entirely attributed to the exchange coupling is still open. The absence of long range magnetic order does not allow direct evaluation of the exchange coupling constants starting from experimental data and so a theoretical determination of these parameters by means of *ab initio* calculations is highly desirable for understanding the behavior of susceptibility in the material. Remarkably, to the best of our knowledge, there is no experimental evidence in the literature of exchange coupling between $J = 0$ ions making the “excess” of susceptibility of Eu_2O_3 a novel puzzle where *ab initio* calculations have the potential of providing interesting evidence toward the solution of this puzzle.

From the theoretical point of view, rare earth compounds represent a challenge for modern electronic structure calculations. Their multiplet structure cannot be explained on the basis of a single Slater determinant. The traditional density functional theory (DFT) methods with local/semilocal approximations to the exchange correlation functionals fail to describe their correlated nature and result in a qualitatively wrong picture with flat f bands accumulated around the Fermi level (E_F). To overcome these problems the LDA + U and the self-interaction corrected local density approximation (SIC-LDA) methods have been widely used in the past. Focusing entirely on Eu^{3+} compounds, LDA + U calculations were performed by Johannes and Pickett¹⁴ on EuN and EuP and by Deniszczyk *et al.*¹⁵ on EuF_3 and EuCo_2X_2 ($X = \text{Si}, \text{Ge}$). SIC-LDA calculations were performed on several rare earth oxides by Petit *et al.*^{16,17} All these works show that the correct physics in these materials can be treated within the LDA + U (SIC-LDA) method. Hence in the present work we compute the electronic and magnetic structure of Eu_2O_3 using the LDA + U approach. Eu being one of the heavy rare earths, the use of an all-electron method is almost essential—in the present work we employ the full-potential linearized augmented plane wave (FLAPW) method¹⁸ implemented within the ELK code.¹⁹ From the corresponding results we obtain very small values for the exchange coupling constants in cubic Eu_2O_3 , which imply a negligible contribution of exchange to the magnetic susceptibility.

II. COMPUTATIONAL DETAILS

The calculations were performed using the ELK code, unless otherwise stated. For the cubic structure a \mathbf{k} -point mesh of $2 \times 2 \times 2$ is used for the Brillouin zone (BZ) integration; given the large dimension of this system (40 atoms per unit cell) and the insulating character of the compound, this choice is a reasonable compromise between accuracy and computational load. For the (smaller unit cell) hexagonal structure, a mesh of $4 \times 4 \times 4$ is used. Spin-orbit coupling has been included in all self-consistent calculations. We have used the fully localized limit of the LDA + U method.²⁰ The values of U for Eu f states and of J are chosen to be 7 and 0.75 eV, respectively.²¹ The contact charge density of the ^{151}Eu nucleus is calculated by modeling the nucleus as a uniformly charged sphere, as described in Ref. 22. A mesh of 259 points to nuclear radius was used. The contact charge density is thus an average of the electronic charge density over the nuclear volume.

The equilibrium structure and the transition pressure were determined using the Vienna Ab-initio Simulation Package (VASP) at absolute zero. The numerical package was applied using the projector augmented-wave pseudopotential (PAW), with a generalized gradient approximation (GGA). The numerical integration of the Brillouin zone was performed using a discrete $4 \times 4 \times 4$ \mathbf{k} -point sampling for the bixbyite structure and a $10 \times 10 \times 8$ \mathbf{k} -point sampling for the hexagonal one. The lattice constants and the internal coordinates of each atom were relaxed simultaneously, using the conjugate gradient method.

III. CRYSTAL AND MAGNETIC STRUCTURE

Eu_2O_3 crystallizes in the cubic bixbyite structure (shown in Fig. 1) with space group $T_h^7 (Ia\bar{3})$; it corresponds to a bcc

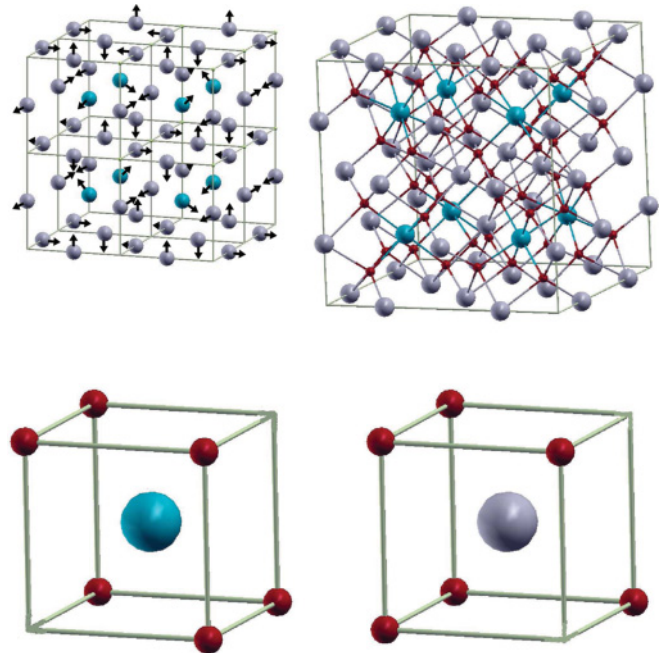


FIG. 1. (Color online) (a) Spin structure of the Er_2O_3 determined using the neutron diffraction²⁴ method. (b) Full structure of cubic Eu_2O_3 . (c) O coordination around Eu_{S_6} sites. (d) O coordination around Eu_{C_2} sites.

lattice with a primitive cell of 40 atoms.²³ Eu atoms occupy the two inequivalent Wyckoff sites $8a$ (site symmetry S_6) and $24d$ (site symmetry C_2), with a distorted octahedral coordination of O atoms (in the $48e$ sites). The experimental lattice constant for Eu_2O_3 is $a = 10.859 \text{ \AA}$.¹¹ The bixbyite structure is derived from a defective cubic fluorite structure, which corresponds to a simple cubic lattice with 10 atoms and half value of the lattice constant. Eu atoms occupy the positions of an fcc lattice; the defective structure is obtained by removing two O atoms at $1/4$ and $3/4$ of the body diagonal. Due to the large number of atoms in the unit cell in the bixbyite structure, Ref. 16 used this smaller, defective fluorite unit cell. In order to compare our results with this work, we have also performed calculations within the defective fluorite unit cell.

In order to evaluate the magnetic exchange coupling constant, the band calculations need to be performed with different configurations of the Eu spins. Experimentally, Eu_2O_3 does not have a long range magnetic order; thus as a starting point we have used the spin configuration of an isostructural Er_2O_3 compound²⁴ (see Fig. 1). This spin configuration also turns out to be stable for Eu_2O_3 in our calculations. However, in this Er_2O_3 -like configuration the sum of the scalar products of the spin of one ion with its nearest-neighbor (NN) spins is always zero, which does not allow for a determination of the NN coupling within a Heisenberg model. In order to obtain a positive sum of scalar products one half of the spins of the C_2 sites have been reversed relative to the Er_2O_3 -like configuration such that all the spins point along the positive direction of the Cartesian x , y , or z axes. In order to compute the exchange couplings we have also studied other ordered phases—to obtain a ferromagnetic (FM)-like state where the direction of the S_6 sites is chosen to maximize the number

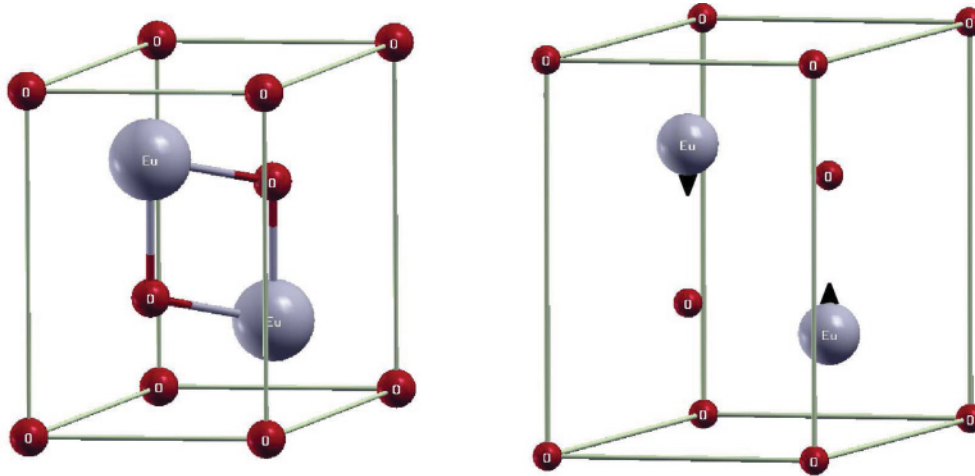


FIG. 2. (Color online) Left panel: High pressure hexagonal structure of Eu_2O_3 . Right panel: Antiferromagnetic configuration of the hexagonal phase.

of positive components, which may be written as $(1,1,1)$, $(1,1,-1)$, $(-1,1,1)$, and $(1,-1,1)$ in the appropriate units; we obtain in this way a positive sum of scalar products for an S_6 or C_2 europium with its twelve NN. In order to obtain an antiferromagnetic (AFM)-like state, the S_6 spin direction is reversed; the sum of products is then negative.

Eu_2O_3 undergoes a structural transition under pressure from the cubic to the hexagonal phase (space group $P\bar{3}m1$)²⁵ (see Fig. 2), which has five atoms per primitive cell (Eu atoms on the Wyckoff positions $2d$ and O atoms on the $2d$ and $1a$ positions).²³ The transition begins at 5 GPa and completes at 13 GPa. At this pressure, the lattice parameters are $a = 3.738 \text{ \AA}$ and $c = 5.632 \text{ \AA}$.²⁵ For this structure, the band calculations are performed with FM as well as AFM spin configuration; in the AFM configuration (shown in Fig. 2), the two cations of the primitive cell have an antiparallel spin orientation.

IV. RESULTS AND DISCUSSION

Before calculating the electronic structure a full structural relaxation is performed using the pseudopotential method and the results are compared with the available experimental data. The atomic positions of the bixbyte structure are described by the u parameter for europium and by the x , y , and z parameters for oxygen;²³ the calculated values are $u = -0.0328$, $x = 0.3877$, $y = 0.1508$, and $z = 0.3813$, which are in good agreement with the experimental ones $u = -0.0313$, $x = 0.3851$, $y = 0.1483$, and $z = 0.3809$.¹¹ The volume dependence of the energy was fitted to the third-order Birch-Murnaghan equation of state;²⁶ the equilibrium lattice constant is $a_0 = 11.02 \text{ \AA}$, which slightly overestimates the experimental value, 10.859 \AA .

The calculated values for the hexagonal structure are $u = 0.2429$ for the Eu parameter and $u = 0.6505$ for the O parameter; no experimental data are available for hexagonal Eu_2O_3 for a comparison. The calculated volume at 13 GPa is $V = 68.13 \text{ \AA}^3$, which agrees well with the experimental one $V_{exp} = 68.15 \text{ \AA}^3$. The estimated pressure of the cubic-hexagonal transition, evaluated by the intersection of the

enthalpy vs pressure curves in the two structures shown in Fig. 3, is $P = 5 \text{ GPa}$. This value is quite consistent with experiments reporting the formation of the hexagonal phase at 5 GPa and a coexistence region of the two phases up to 13 GPa, at room temperature.

Due to the large size of the bixbyte unit cell, the calculations with the FLAPW method of the energy vs volume have been performed using the defective fluorite cell with a FM configuration. The volume dependence of the energy was fitted to the third-order Birch-Murnaghan equation of state.²⁶ We obtain an equilibrium lattice constant $a_0 = 10.622 \text{ \AA}$, 2% smaller than the experimental value (consistent with the typical error in LDA or LDA + U calculations). The calculated bulk modulus $B_0 = 140 \text{ GPa}$ is also in good agreement with the experimental value of $B_{0,exp} = 145 \pm 2 \text{ GPa}$ (Ref. 25) (measured in the bixbyte phase).

As mentioned earlier, the first problem in the study of this system is the choice of spin configuration, since experiments do not report any magnetic order in this $J = 0$ system. We therefore assume as a starting (reference) configuration the experimental magnetic structure of isostructural Er_2O_3 . In this configuration, spin moments are not collinear, and the two

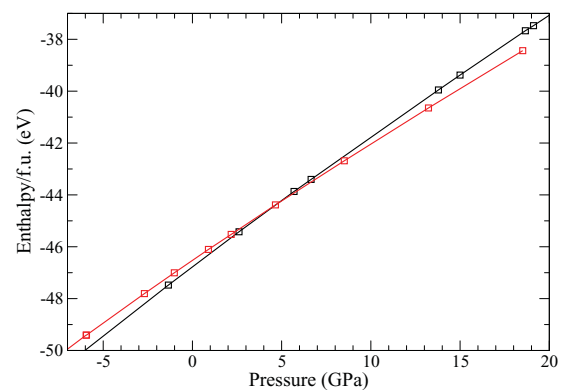


FIG. 3. (Color online) Enthalpy vs pressure for the cubic structure (black) and the hexagonal one (red/gray). The squares point out the calculated values; the line is a guide for the eye.

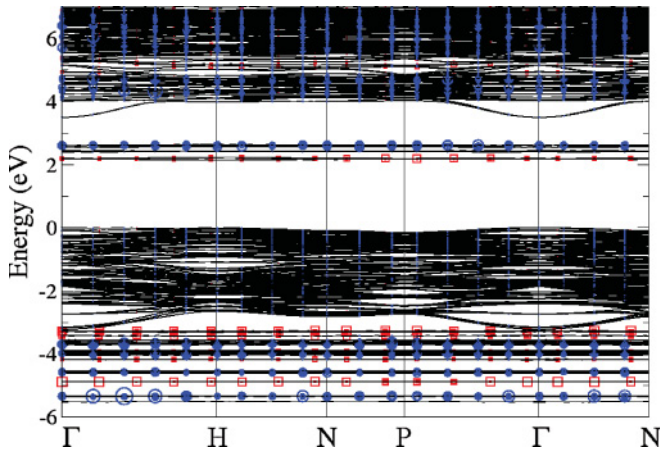


FIG. 4. (Color online) Band structures of cubic Eu_2O_3 along the symmetry directions of the Brillouin zone. Eu $4f$ character is denoted by red squares and blue circles for the S_6 and C_2 sites, respectively.

crystallographic sites have totally different directions:²⁴ while the S_6 moments are directed along the diagonal axes, C_2 sites direct their spin along the Cartesian axes (see Fig. 1).

The band structure of cubic Eu_2O_3 with the Er_2O_3 -like spin configuration is shown in Fig. 4. The red squares and blue circles in Fig. 4 represent the importance of the contribution from Eu $4f$ states, for sites S_6 and C_2 , respectively. The general features of Eu_2O_3 bands can be readily explained as follows: the O p states are responsible for the bands located in the energy region between ≈ -3 eV and the Fermi level (which is the zero of energy in all our plots). The Eu^{3+} ions are in a $4f^6$ configuration, which leaves an empty $4f$ orbital per atom in the majority spin channel. Minority $4f$ states, on the other hand, are completely empty and form the group of bands from $+4$ to $+8$ eV. Occupied majority spin $4f$ states form the group of 24 bands sitting from -5.5 to -3 eV and their splitting into four separated groups is similar to the situation in Eu pnictides.¹⁴ This splitting in the case of Eu pnictides was interpreted as an effect of the intra-atomic anisotropic exchange—a test calculation based on LDA resulted in a single narrow f manifold indicating that splitting cannot originate from crystal field effects, making the complex exchange effect in this open shell system the most likely explanation. The large distance between (equal spin) filled and empty counterparts derives from the large U value for localized $4f$ states. The empty majority spin states lie around 2.3 eV above E_F . This electronic structure therefore reflects the electronic configuration of the Eu^{3+} ions. All the $4f$ bands have a negligible dispersion (≈ 0.2 eV), consistent with the localized nature of these orbitals.

For better understanding of the electronic states presented in Fig. 5 are the densities of states (DOS) of cubic Eu_2O_3 in the Er_2O_3 -like spin configuration. Figure 5 confirms the picture given above. In particular, the states from -3 eV to E_F derive from O states and hybridize only weakly with Eu states. Besides $4f$ states, Eu's most prominent contribution to the electronic structure is the $5d$ states, mostly located in the conduction band region above 4 eV. The narrow peaks from -5.5 to -3 eV and the structures above 4 eV are derived from filled majority and empty minority Eu $4f$ states,

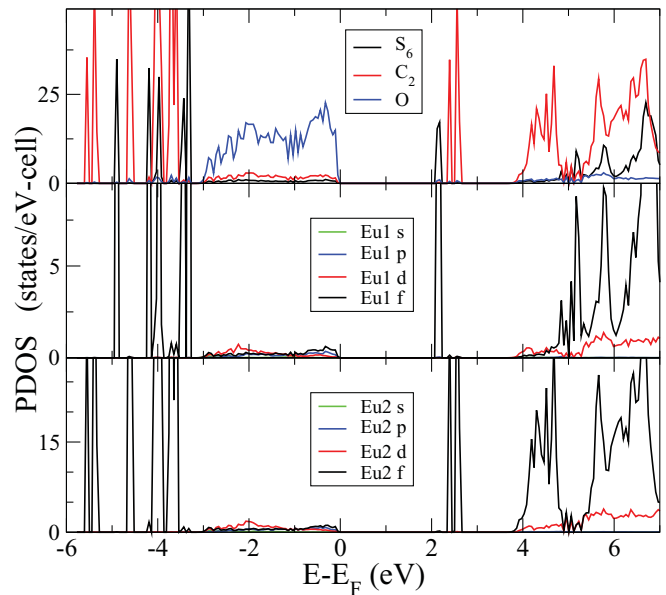


FIG. 5. (Color online) Orbital projected DOS of cubic Eu_2O_3 per primitive cell in the Er_2O_3 -like configuration. The Eu1 and Eu2 labels indicate the S_6 and C_2 sites, respectively.

respectively. The peaks in the region ≈ 2 – 2.5 eV above E_F are predominantly Eu states (in particular, empty majority spin $4f$ states), with a very small contribution from oxygen orbitals. The marginal Eu $4f$ –O $2p$ hybridization indicates a small value of the NN exchange coupling.

The importance of the crystal field (CF) effects in this compound has been a subject of discussion in the past.^{4,6} Optical measurements have been interpreted assuming that the S_6 and C_2 sites have a very different CF splitting. Our results support this interpretation (see Fig. 5) and show that the f states behave differently for the two sites—the lower symmetry of the C_2 site results in a larger subdivision of the $4f$ peaks with occupied f states shifted 0.5 eV lower in energy compared to the occupied f states with S_6 site symmetry. The unoccupied f states show a similar behavior with C_2 site symmetry states moved higher in energy with respect to S_6 site projected f states. This leads to the C_2 site having a much larger energy gap between occupied and empty majority spin states as compared to the S_6 site, which in turn implies different density matrices for the two sites. This difference can be related to the different expectation values of orbital momentum (to be discussed later).

In order to understand the exchange interaction in Eu_2O_3 we studied two further spin arrangements, referred to as FM and AFM configurations (we refer to Sec. III for their description). In Fig. 6 we compare the DOS for Eu_2O_3 in the FM and AFM configurations. It is clear that spin ordering affects the Eu states marginally and the corresponding DOS are almost identical. These results have consequences on the exchange parameters as the total energy difference between these two configurations is very small.

As stated above, band structure methods have strong limitations in calculations of rare earth compounds, in particular in dealing with the spin and orbital angular momenta. Following the usual procedure described in Ref. 14 for the case of the

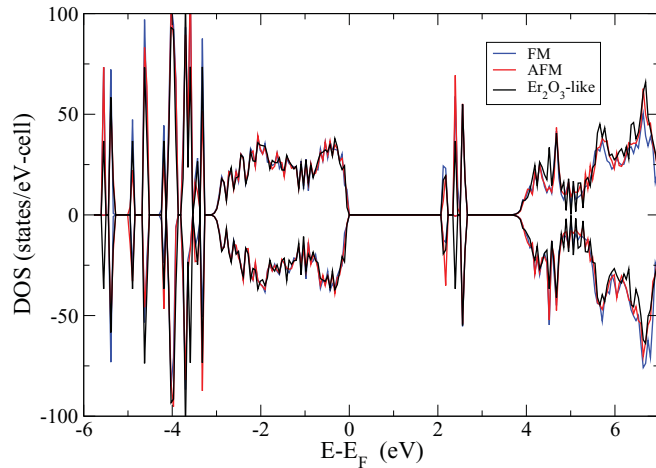


FIG. 6. (Color online) Total DOS of cubic Eu_2O_3 in the Er_2O_3 -like configuration and in the two (FM and AFM) configurations described in the text.

trivalent Eu ion, we assign a direction (local α axis) to \mathbf{S} and \mathbf{L} and deal with the projections S_α and L_α on this axis. While this representation does not reproduce the experimental situation (where the projections of \mathbf{S} and \mathbf{L} vanish on any given direction), it is the closest approximation we can have of the physical reality within our scheme. The local axes are different for the two sites: in the case of C_2 it points along the Cartesian axes, and in the S_6 site it points along the main cube diagonal. In units of \hbar we obtain for the S_6 site $S_\alpha = 2.77$, $L_\alpha = -1.56$, and $J_\alpha = 1.21$. Our value of S_α differs from the expected value $S_\alpha = 3$ for the free ion probably because of the use of muffin-tin sphere for computing integrals and also because of an incomplete spin polarization. In the case of the C_2 site, on the other hand, we get very different results: the components along the corresponding local axes α' are $S_{\alpha'} = 2.41$, $L_{\alpha'} = -2.34$, and $J_{\alpha'} = 0.07$. In other words, the $J = 0$ ground state of Eu seems to be reproduced to a much larger extent. Again (consistent with experiments) we find very different behaviors for the two sites. We should mention that our small value of L_α for the S_6 site is similar to the value $L_\alpha = -1.5$ obtained in EuN by Johannes and Pickett,¹⁴ who ascribed this result to an overquenching of angular momentum caused by an overestimated crystal field effect within DFT.

At this point it is interesting to compare the electronic structures of Eu_2O_3 and EuN (Ref. 14) (which crystallizes in the rock salt structure and corresponds to an Eu^{3+} configuration). The general features of the band structures are quite similar, apart from obvious differences associated with the different ligand (the center of gravity of O $2p$ states lies slightly deeper in energy). A qualitative difference exists in the properties of Eu_2O_3 and EuN: EuN is metallic in nature and this metallic character arises from partially occupied dispersed Eu $5d$ bands, crossing the empty majority $4f$ bands. On the other hand in the case of Eu_2O_3 similar dispersed bands with Eu $5d$ contribution exist but they also have a relevant interstitial character and lie above the empty majority $4f$ bands; as a consequence, Eu_2O_3 turns out to be an insulator. It is interesting to notice that both in our calculations for the simplified structure suggested by Petit *et al.*¹⁶ and in their SIC calculations these bands cross

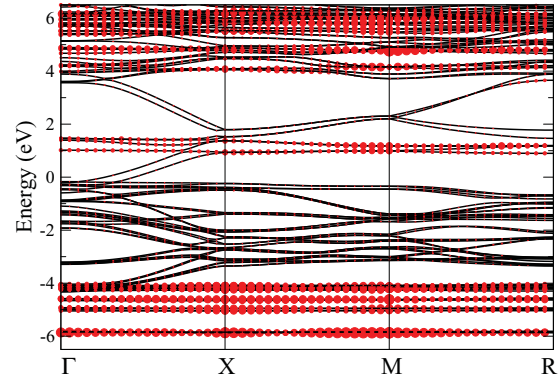


FIG. 7. (Color online) Bands of Eu_2O_3 in the simplified structure (defective cubic fluorite cell) in the FM configuration. The $4f$ character is denoted by red circles.

E_F and in contrast with experiments give a spurious metallic character to Eu_2O_3 , as shown in Fig. 7. The origin of the difference in character between the bixbyte and the simplified structure partially lies in the relaxation around the vacancies, which is not allowed by symmetry in the latter. In fact, an inspection of the charge corresponding to these dispersed bands in the simplified structure shows that these bands derive from quantum states localized in the O vacancy sites. However, test calculations have shown differences among the bands of the two compounds which are not accounted for by simple local atomic relaxation. As a matter of fact, we notice that the simplified structure is not entirely equivalent to the structure of the bixbyte (for instance, only one of the two inequivalent Eu sites is found in the simplified structure) and that the full structure has to be used to properly describe this system.

Under pressure Eu_2O_3 undergoes a structural phase transition to a hexagonal phase (see Fig. 2). Due to the very large computational load involved, the calculation of the transition pressure is out of the scope of the present investigation. However, we minimized the total energy of Eu_2O_3 in the hexagonal phase. The fitted energy minimum is at $V_0 = 67.62 \text{ \AA}^3$, and $B_0 = 180 \text{ GPa}$. The calculated bulk modulus compares well with the experimental value $B_{0,exp} = 151 \pm 6 \text{ GPa}$,²⁵ As for the equilibrium volume, the experimental hexagonal volume is $V_{exp} = 68.15 \text{ \AA}^3$ when the transition is completed (at 13.1 GPa),²⁵ Using the theoretical bulk modulus, we arrive at an equilibrium volume at 13.1 GPa equal to 62.7 \AA^3 , which underestimates the experimental lattice constant by about 2.8% (which is typical of LDA-based functionals).

In order to understand how pressure modifies the electronic structure of this compound, we have studied its properties in the hexagonal phase, at the lattice parameters corresponding to $P = 13.1 \text{ GPa}$. The band structure of the hexagonal Eu_2O_3 is shown in Fig. 8 for both FM and AFM configurations. The general features of the bands are similar to the cubic phase; hexagonal Eu_2O_3 is a semiconductor, with a gap of 2.3 eV between the valence and the unoccupied $4f$ band, and a gap of 4.1 eV between the valence and the conduction band. This semiconducting behavior is in agreement with the experimental optical and transport properties of Eu_2O_3 . In contrast to the cubic phase, in the hexagonal phase the dispersed band with the minimum around 3.5 eV at the Γ

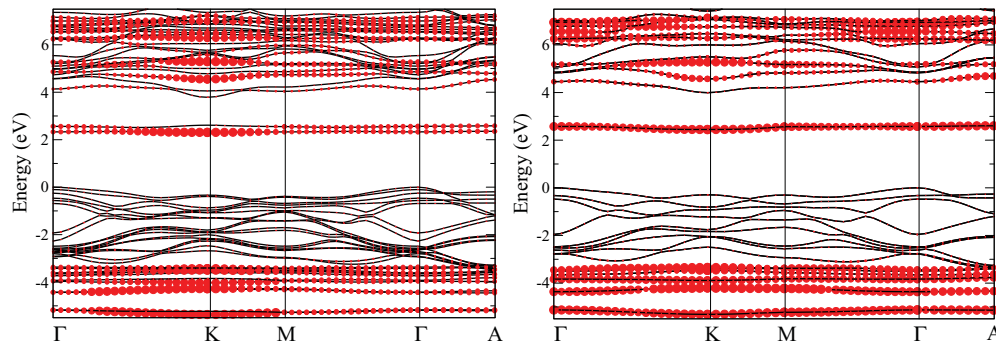


FIG. 8. (Color online) Band structures of hexagonal Eu_2O_3 in the primitive cell. Left panel: FM state. Right panel: AFM state. Eu 4f character is denoted by red circles.

point is not present. This difference may be related to the fact that the hexagonal structure has no vacancies in the atomic O positions, ruling out the possibility of having bands with a large interstitial character.

The total DOS of cubic and hexagonal Eu_2O_3 are presented in Fig. 9. While the structure of Eu_2O_3 levels is similar, the O 2p states have a larger bandwidth and overlap with the occupied Eu 4f manifold. This increase of the O 2p bandwidth is clearly a consequence of the compression O atoms experience under pressure. Also, the exchange-related splitting of the 4f levels is different in the cubic and hexagonal phases.

Some results of our calculations on cubic Eu_2O_3 may be compared with experimental values. The gap between the valence and the conduction band ($\Delta E_{v \rightarrow c}$) has been obtained by optical measurements; the calculated value $\Delta E_{v \rightarrow c} = 3.50$ eV is close to the experimental one²⁷ $\Delta E_{opt} = 4.3 \pm 0.3$ eV. The gap between the valence and the empty majority spin Eu f band has been determined by the experimental curve of conductivity vs temperature; the calculated value $\Delta E_{v \rightarrow f} = 2.18$ eV is in reasonable agreement with the experimental value²⁸ of $\Delta E_{cond} = 1.84$ eV.

Our calculations allow us to calculate the electron density on the nucleus or contact charge density, which is relevant in the context of the Mössbauer spectroscopy of ^{151}Eu in cubic Eu_2O_3 . The electron density on the nucleus $\rho(0)$ may be evaluated in terms of the difference $\Delta\rho(0) = \rho(0) - \rho_{\text{EuF}_3}(0)$

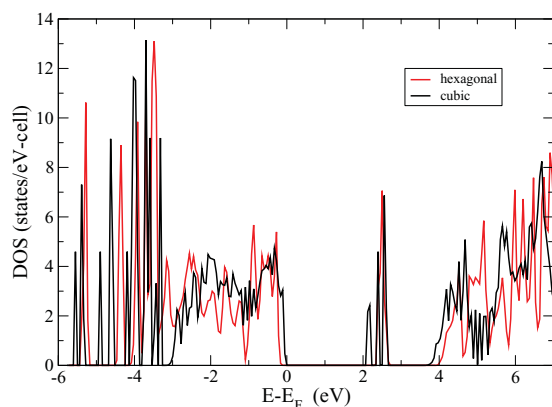


FIG. 9. (Color online) Total DOS of cubic and hexagonal Eu_2O_3 in the FM state.

relative to tetragonal EuF_3 , which is the reference compound. Using the experimental isomer shift¹² $\delta = 1.03 \pm 0.01$ mm/s and the differential nuclear radius of Ref. 29, we find an experimental density difference to be $\Delta\rho(0) = 3.18 \pm 0.03 a_0^{-3}$; the calculated value for the dominating C_2 site is $\Delta\rho(0) = 3.17 a_0^{-3}$ which is in very good agreement with the experimental value.

In order to verify our general capability of computing contact charge densities in different environments, we performed calculations in other related systems: EuF_3 , the most ionic compound with trivalent europium, EuF_2 , the most ionic divalent compound (cubic fluorite structure), and divalent oxide EuO (rocksalt structure). The calculated charge density difference is $\Delta\rho(0) = -34.93 a_0^{-3}$ for EuO , to be compared with the experimental value²⁹ $\Delta\rho(0) = -37.91 \pm 0.04 a_0^{-3}$; for EuF_2 the calculated value is $\Delta\rho(0) = -40.70 a_0^{-3}$, in good agreement with the experimental one²⁹ $\Delta\rho(0) = -41.93 \pm 0.04 a_0^{-3}$.

V. EXCHANGE INTERACTIONS

The exchange interaction in ions with $L \neq 0$ is characterized by the dependence of the exchange integral on orbital orientation. According to Van Vleck and Huang³⁰ this effect gives rise to an “anisotropic exchange,” resulting from the dependence of orbital charge density on the direction. The coupling between the ions i and j may still be described by the exchange potential $V_{ex,ij}$, as demonstrated in Ref. 30: the exchange coupling for Eu^{3+} ions in their ground state and in cubic compounds may be written in the standard form

$$V_{ex,ij} = -2a_{eff}^{(ij)} \mathbf{S}_i \cdot \mathbf{S}_j \quad (1)$$

where \mathbf{S}_i is the spin of the ion i and $a_{eff}^{(ij)}$ are the effective exchange constants. In other words, we can use the standard form of the isotropic coupling to deal with an anisotropic exchange. Therefore, it is possible to determine the $a_{eff}^{(ij)}$ constants by calculating the energies of different spin configurations. These constants allow us to determine the effect of the exchange coupling on the magnetic susceptibility.

Our results show that there is no significant total energy difference between the FM-like and the AFM-like phases (for their definition see Sec. III), with an energy convergence parameter $\epsilon \sim 3 \times 10^{-4}$ eV and a total energy $E_t \sim 5 \times 10^6$ eV. The maximum possible strength of the exchange

coupling consistent with these results corresponds to an energy difference per primitive cell $\Delta E_i \sim 2\epsilon$, which leads to a difference per Eu atom of $\Delta E \sim 0.04$ meV. In this work we consider only the exchange coupling of the Eu^{3+} ion with its 12 NN, since it is expected to be the largest. In fact, in the bixbyite structure, NN exchange is mediated by the oxygen atom, which is not the case for next NN Eu atoms. With this assumption, the effective exchange constants refer only to the coupling of NN Eu ions. We also assume that all the NN pairs have the same $a_{eff}^{(ij)} = a_{eff}$. Starting from the energy difference $\Delta E \sim 0.04$ meV and the spin values given by our calculations, we obtain that the upper bound of the effective exchange constant is $a_{eff} \sim 0.002$ meV.

Due to a lack of long range magnetic order,³¹ the value of a_{eff} cannot be verified by direct comparison with experimental magnetic data. However, this interaction may give a contribution to the magnetic susceptibility. According to Ref. 4, the magnetic susceptibility χ may be written as

$$\chi = \chi_{dia} + \chi_p = \chi_{dia} + \chi_{VV} + \chi_{ex}, \quad (2)$$

where the paramagnetic susceptibility χ_p , obtained by subtraction of the diamagnetic core component χ_{dia} , is the sum of the Van Vleck contribution χ_{VV} and of the exchange contribution χ_{ex} .⁴ At $T = 0$ K,

$$\chi_{VV} = \frac{8N\mu_B^2}{3K_B} \sum_{k=1}^3 \frac{1}{E_{1k}}, \quad (3)$$

$$\chi_{ex} = \frac{128N\mu_B^2 A_{eff}}{E_1(E_1 - 16A_{eff})}, \quad (4)$$

where N is the number of atoms, μ_B is the Bohr's magneton, K_B is the Boltzmann's constant, E_{1k} are the energies of the triplet state 7F_1 centered around the energy E_1 , and

$$A_{eff} = \sum_{j=1}^{12} a_{eff}^{(ij)} = 12a_{eff}. \quad (5)$$

However, the contribution of the S_6 and C_2 sites must be evaluated separately, because the energies of the 7F_1 state are different. Since the multiplet energies are not accessible from our one-particle calculations, we calculate the Van Vleck contribution by using the experimental optical energies for the two sites given by Ref. 6; we get $\chi_{VV}^{(exp)} = 7.72 \times 10^{-3}$ cm³/mol of Eu (in CGS units). If we subtract this contribution from the experimental value of the paramagnetic susceptibility $\chi_p^{(exp)} = 9.1 \times 10^{-3}$ cm³/mol of Eu (in CGS units) of Ref. 3, we obtain the value of the excess susceptibility $\Delta\chi = \chi_p - \chi_{VV} = 1.38 \times 10^{-3}$ cm³/mol of Eu.

In accordance with Van Vleck and Huang,^{4,30} if we assume that this excess susceptibility is due to the exchange contribution only ($\Delta\chi = \chi_{ex}$) and that A_{eff} is equal for both sites, we can estimate the experimental value of $A_{eff} = 0.41$ meV. By using the maximum value of a_{eff} obtained by our band calculations, we obtain a theoretical upper bound for the constant to be $A_{eff} \sim 0.02$ meV. Our results, therefore, lead to the conclusion that in cubic Eu_2O_3 the difference between the experimental paramagnetic susceptibility and the Van Vleck contribution cannot be due to the contribution of the exchange

interaction, in contrast with the conclusions of Van Vleck and Huang.^{4,30} It is consistent, on the other hand, with the fact that the experimental susceptibility (per mole of Eu) does not decrease in the solid solutions of Eu_2O_3 into A_2O_3 . The point of view of Van Vleck and Huang has also been criticized before by Caro and Porcher,¹³ who performed a calculation of the Van Vleck contribution χ_{VV} including the matrix elements among atomic wave functions of the Eu 4*f* states. They obtained a resulting χ_p in good agreement with experimental values, without invoking any contribution from the exchange interaction. Our calculations are also consistent with these results.

The investigation of the exchange interaction has also been performed for the hexagonal phase of Eu_2O_3 under pressure. In this case, Eq. (1) is not applicable, because the structure of the compound is not cubic; therefore, it is not possible to determine the exchange constants by total energy differences. In contrast to the cubic phase in the case of the hexagonal structure the application of a weak magnetic field along the *c* axis gives collinear spins. In the AFM configuration (described in Sec. III) the cation spins have parallel orientation in planes perpendicular to the magnetic field direction (*z* axis), with antiparallel orientation between planes. The Eu atom has three neighbors at 3.50 Å in the lower plane, three at 3.59 Å in the upper plane, and four neighbors at a distance of 3.74 Å in the same plane.^{23,25} The energy difference per Eu atom is $E_{AFM} - E_{FM} = -3.63$ meV. Therefore in the hexagonal structure we obtain a nonnegligible AFM exchange interaction between the Eu ion and its six NN. Interestingly the energy difference is of the same order of magnitude as that found by Johannes and Pickett for EuN and EuP.¹⁴

The exchange interaction is about 100 times stronger in the hexagonal phase than in the cubic one. As a first guess, one might attribute this difference to the shorter Eu-Eu distance in the hexagonal phase ($d_{\text{Eu-Eu}}$ is 3.50–3.74 Å in the hexagonal phase and 3.84 Å in the cubic one). To verify this possibility, we performed test calculations in the hexagonal structure, changing the lattice constant so as to match the interatomic Eu-Eu distance of the cubic phase. The corresponding exchange coupling did not decrease sufficiently to support this view. The rationale for the different couplings may probably be found in the different local O coordination around Eu ions, as the oxygen orbitals mediate the Eu-Eu interaction: in the hexagonal structure there are two O atoms binding two NN Eu ions, while there is only one intermediate O atom in the cubic one. An analysis of the partial densities of states in the two structures supports this view, with a quite large hybridization of Eu 4*f* and O orbitals in the hexagonal phase. Interestingly, we also observe that the phase with stronger exchange coupling has a collinear spin structure, while the structure with weaker interaction is characterized by noncollinear spins.

VI. CONCLUSION

In conclusion, we have studied the electronic structure of cubic bixbyite Eu_2O_3 and its high pressure hexagonal phase by means of FLAPW calculations within the LDA + *U* method. In both phases the filled O 2*p* and empty majority spin Eu 4*f* states are separated by an ≈ 2.1 -eV gap, while minority Eu 4*f* states start around 4 eV above E_F , in agreement with

the optical and transport measurements.^{27,28} The calculated contact charge density agrees with the experiment.

A full structural relaxation, performed with the pseudopotential method, is in agreement with the experiment, in particular, the pressure of the cubic-hexagonal transition and the presence of a coexistence region where correctly evaluated.

From the comparison of FM and AFM calculations we infer that the interatomic exchange interaction is negligible in cubic Eu_2O_3 and so is its effect on the susceptibility. This is consistent with the experimental observation of a constant susceptibility (per mole of Eu) of solid solutions of Eu_2O_3 into A_2O_3 ($A = \text{Y, Lu, Sc}$). Our calculations are in contrast with the point of view of Van Vleck and Huang,^{4,30} according to which exchange is needed to explain the behavior

of the magnetic susceptibility. Our results are consistent with later calculations,¹³ which could explain the experimental susceptibility by including the matrix element in the Van Vleck contribution. In the hexagonal phase we observe the presence of a small but significant AFM exchange interaction between the Eu ion and its six NN. Therefore, in this phase we could have a non-negligible contribution of exchange to the magnetic susceptibility, but for now no experimental measurements are available for comparison.

ACKNOWLEDGMENTS

SM thanks M. D. Johannes for useful discussions. This work was partially supported by a computing grant from CINECA (Italy).

*giorgio.concas@dsf.unica.it

¹A. S. Borovik-Romanov and N. M. Kreines, *Sov. Phys. JETP-USSR* **2**, 657 (1956).

²B. Antic, M. Mitric, and D. Rodic, *J. Phys. Condens. Matter* **9**, 365 (1997).

³G. Concas, G. Spano, M. Bettinelli, and A. Speghini, *Z. Naturforsch., A: Phys. Sci.* **63**, 210 (2008).

⁴N. L. Huang and J. H. Van Vleck, *J. Appl. Phys.* **40**, 1144 (1969).

⁵N. C. Chang and J. B. Gruber, *J. Chem. Phys.* **41**, 3227 (1964).

⁶M. Buijs, A. Meyerink, and G. Blasse, *J. Lumin.* **37**, 9 (1987).

⁷A. Grill and M. Schieber, *Phys. Rev. B* **1**, 2241 (1970).

⁸S. Kern and R. Kostecky, *J. Appl. Phys.* **42**, 1773 (1971).

⁹O. L. Malta, E. Antic-Fidancev, M. Lemaitre-Blaise, A. Milicic-Tang, and M. Taïbi, *J. Alloys Compd.* **228**, 41 (1995).

¹⁰E. Zych, *J. Phys. Condens. Matter* **14**, 5637 (2002).

¹¹F. Hanic, M. Harmanova, G. G. Knab, A. Urusovskaya, and K. S. Bagdasrov, *Acta Crystallogr. Sect. B* **40**, 76 (1984).

¹²G. Concas, G. Spano, M. Bettinelli, and A. Speghini, *Z. Naturforsch., A: Phys. Sci.* **58**, 551 (2003).

¹³P. Caro and P. Porcher, *J. Magn. Magn. Mater.* **58**, 61 (1986).

¹⁴M. D. Johannes and W. E. Pickett, *Phys. Rev. B* **72**, 195116 (2005).

¹⁵J. Deniszczuk, W. Burian, P. Maslankiewicz, and J. Szade, *J. Alloys Compd.* **442**, 239 (2007).

¹⁶L. Petit, A. Svane, Z. Szotek, and W. M. Temmerman, *Phys. Rev. B* **72**, 205118 (2005).

¹⁷L. Petit, A. Svane, Z. Szotek, and W. M. Temmerman, *Top. Appl. Phys.* **106**, 331 (2007).

¹⁸D. J. Singh and L. Nordstrom, *Planewaves, Pseudopotentials, and the LAPW Method* (Springer, New York, 2006).

¹⁹J. K. Dewhurst, S. Sharma, L. Nordstrom, F. Cricchio, and F. Bultmark, *The Elk Code Manual* [<http://elk.sourceforge.net/>].

²⁰A. G. Petukhov, I. I. Mazin, L. Chioncel, and A. I. Lichtenstein, *Phys. Rev. B* **67**, 153106 (2003).

²¹J. Kunes and R. Laskowski, *Phys. Rev. B* **70**, 174415 (2004).

²²S. Sharma, J. K. Dewhurst, L. Nordström, and B. Johansson, *J. Phys. Condens. Matter* **14**, 3537 (2002).

²³R. W. G. Wyckoff, *Crystal Structures* (Interscience Publishers, New York, 1964), Vol. 2.

²⁴R. M. Moon, W. C. Koehler, H. R. Child, and L. J. Raubenheimer, *Phys. Rev.* **176**, 722 (1968).

²⁵Jiang Sheng, Bai Li-Gang, Liu Jing, Xiao Wan-Sheng, Li Xiao-Dong, Li Yan-Chun, Tang Ling-Yun, Zhang Yu-Feng, Zhang De Chun, and Zheng Li-Rong, *Chin. Phys. Lett.* **26**, 76101 (2009).

²⁶F. Birch, *J. Geophys. Res.* **83**, 1257 (1978).

²⁷A. V. Prokofiev, A. I. Shelykh, and B. T. Melekh, *J. Alloys Compd.* **242**, 41 (1996).

²⁸H. B. Lal and K. Gaur, *J. Mater. Sci.* **23**, 919 (1988).

²⁹G. K. Shenoy, in *Mössbauer Spectroscopy Applied to Inorganic Chemistry*, edited by G. J. Long (Plenum Press, New York, 1984), Vol. 1, p. 57.

³⁰J. H. Van Vleck and N. L. Huang, in *Polarisation, Matière et Rayonnement*, edited by Societe Francaise de Physique (University Presses of France, Paris, 1969), p. 507.

³¹A. H. Morrish, *The Physical Principles of Magnetism* (IEEE, New York, 2001).